Rheological characterization of Polyanionic Cellulose solutions with application to drilling fluids and cuttings transport modeling

Alexander Busch[1,*], Velaug Myrseth[2], Milad Khatibi[3], Paal Skjetne[4], Sigve Hovda[1], Stein Tore Johansen[1,4]

[1] Norwegian University of Science and Technology (NTNU), Trondheim, Norway
[2] SINTEF Petroleum Research AS, Bergen, Norway
[3] University of Stavanger (UiS), Stavanger, Norway
[4] SINTEF Materials and Chemistry, Trondheim, Norway

*Corresponding author: alexander.busch@ntnu.no, alexander.busch@alumni.ntnu.no

Keywords: Rheological characterization, Modeling, CFD, Cuttings transport, Flow curves, Thixotropy, Viscoelasticity, Uncertainty, Time scales.

Abstract

In petroleum drilling, aqueous Polyanionic Cellulose solutions (PAC) are often used as a drilling fluid model system in experimental laboratory studies to investigate cuttings transport. Cuttings transport refers to the transportation of drilled-off solids out of the wellbore. In these studies, PAC solutions are typically assumed to behave purely viscous, i.e. they do not show time-dependent/thixotropic and/or viscoelastic properties. In this study, a rheological characterization of PAC has been performed in combination with an evaluation of time scales characterizing the fluid to verify the conventional assumption of a purely-viscous fluid. It is found that PAC solutions are generally not purely viscous; they feature viscoelastic behavior on time scales of the order of 0.01 to 1 s, such as normal stress differences, as well as thixotropic behavior on larger time scales of the order of 10 to 1000 s because of their polymeric microstructure. If simplified to a purely viscous fluid, the degree of uncertainty in representing the measured apparent shear viscosity may increase by an order of ≈ 75 to 90% depending on the relevant time scale. When obtaining flow curves, a sufficiently long measurement point duration (sample time for a particular torque reading) is required to ensure that the liquid microstructure has reached its dynamic equilibrium at the desired shear rate. Due to their polymeric nature, PAC solutions feature Newtonian viscosity plateaus at both low and high shear rates. For modeling purposes, the application of a Cross/Carreau material function is recommended because it both best describes the flow curve data and minimizes extrapolation errors compared to the conventionally used Power Law material function.

Nomenclature

Greek symbols

γ	Strain.
$\dot{\gamma}$	Shear rate, total shear measure, $\dot{\gamma} = \frac{\partial u}{\partial y} = \frac{\partial \gamma}{\partial t}$ for simple shear flow.
δ	Difference.
ϵ	Ratio of rheological and observation time scale.
η	Apparent shear viscosity.
λ	Rheological time scale.
μ	Newtonian shear viscosity.
ρ	Density.
Ψ	First Normal Stress Coefficient.
ω	Frequency.
θ	Fann viscometer speed.
ϕ	Phase shift angle.

Latin symbols

$\mathbf{D}$	Rate of deformation tensor.
g	Gravity.
G	Modulus.
N	Normal stress difference.
p	Pressure.
T	Transposed, Torque.
$\mathbf{T}$	Stress tensor.
$\mathbf{u}$	Velocity.
y	Rheometer gap size.

Indices

0	Zero, $\dot{\gamma} \to 0$.
$*$	Complex.
'	Storage modulus.
''	Loss modulus.
∞	Infinity, $\dot{\gamma} \to \infty$.
Ca	Carreau.
Cr	Cross.
FNSD	First Normal Stress Difference.
i, j	Einstein Notation Index.
Max	Maxwell.
PL	Power Law.
r	Relative.
RS	Recoverable Shear.

Abbreviations

3ITT	3-Intervall-Thixotropy-Test.
AS	Amplitude Sweep.
CFD	Computational Fluid Dynamics.

CMC	Carboxymethyl Cellulose.
CSR	Controlled Shear Rate.
CSS	Controlled Shear Stress.
DR	Drag Reduction.
FC	Flow Curve.
FNSC	First Normal Stress Coefficient.
FNSD	First Normal Stress Difference.
FS	Frequency Sweep.
GNF	Generalized Newtonian Fluid.
HB	Herschel-Bulkley.
MPD	Measurement Point Duration.
ORO	Oscillation-Rotation-Oscillation.
PAC	Polyanionic Cellulose.
PL	Power Law.
RS	Recoverable Shear.
RRR	Rotation-Rotation-Rotation.
SD	Standard Deviation.
SE	Standard Error.

1 Introduction

Polyanionic Cellulose (PAC) is frequently used as drilling fluid viscosifier in oil drilling [1–6] and, dissolved in distilled water, as drilling fluid substitute in cuttings transport studies [7–16] or other multiphase flow studies [17–19] relevant to the oil & gas industry. Cuttings transport is the process of adequately flushing drilled-off solids ("cuttings") out of a petroleum wellbore. Inadequate flushing of cuttings from the bore hole (poor hole cleaning) leads to accumulation of solids in the wellbore. Problems associated with cuttings transport are a major contributor to downtime during drilling operations. In drilling fluids, PAC may act as a loss agent (preventing loss of drilling fluids into permeable formations) as well as a viscosifying agent (developing viscosity depending on concentration and other variables such as water chemistry and salinity). In laboratory studies of cuttings transport, PAC is used as a drilling fluid substitute, i.e. a drilling fluid model system, since it yields transparent, non-hazardous, shear-thinning fluids when added to (distilled) water. The translucency allows for optical investigations of the flow as well as optical measurement techniques such as particle image velocimetry.

The relationship between experimental cuttings transport studies in a laboratory, the real drilling process (cuttings transport in a wellbore), and cuttings transport modeling as well as the role of rheometric testing is conceptually depicted in Figure 1. PAC may be used both in the real drilling process, e.g. as a viscosifying agent, and/or in an experimental study in a laboratory as a test fluid modeling the real drilling fluid. Numerical modeling of cuttings transport using e.g. Computational Fluid Dynamics (CFD) methods[1] is another methodology, which may be used to investigate cuttings transport, or more generic, multiphase problems. CFD results are usually validated against experimental data generated in the laboratory. CFD models require a constitutive equation[2] describing the fluid's rheology. In the petroleum industry, both on engineering and research level, drilling fluids in 3D CFD cuttings transport studies are typically modeled as incompressible and purely viscous, i.e. Generalized Newtonian Fluids (GNF), where the stress tensor of the Cauchy equations of motion is given as

$$\mathbf{T} = -p\mathbf{I} + 2\eta\left(\dot{\gamma}\right)\mathbf{D} \tag{1}$$

where $\mathbf{D}$ is the rate of deformation tensor

$$\mathbf{D} = \frac{1}{2}\left[\nabla\mathbf{u}_i + (\nabla\mathbf{u}_j)^T\right] \tag{2}$$

and the shear rate $\dot{\gamma}$ is a total shear measure defined as

$$\dot{\gamma} = \sqrt{2\mathbf{D}:\mathbf{D}} \tag{3}$$

In equation (1), the apparent dynamic shear viscosity $\eta(\dot{\gamma})$ of the fluid may be a function of the shear rate $\dot{\gamma}$ or, in case of Newtonian fluids, constant. Commonly used models in the drilling industry to represent $\eta(\dot{\gamma})$ are the Bingham model [20] (accounting for yield stress phenomena), the Ostwald/de Waele "Power law" (PL) [21] (accounting for shear-thinning behavior) or the Herschel-Bulkley (HB) model [22] being a combination of the former two. More sophisticated models such as the Cross [23] or Carreau [24] models (accounting for limiting viscosities at both low and highs shear rates) are used on a very limited basis. Higher-order fluid descriptions, i.e. constitutive equations accounting for time-dependent and/or viscoelastic behavior, have - to the awareness of the authors - not been applied in CFD cuttings transport studies.

The selection of a particular type of material function for the apparent viscosity $\eta(\dot{\gamma})$ is based on the particular rheometric data available. A rheological model for the fluid under consideration is built by fitting the material function to the rheometric data in order to obtain numerical values for the corresponding model coefficients. Rheometric data is obtained from rheometric testing, e.g. obtaining value pairs of the apparent viscosity vs. shear rate in case of a GNF, for the fluids used in the experiment. Alternatively, one may deduce rheometric data from available experimental pressure loss

[1] CFD methods are hereafter considered as multiphase finite volume Reynolds Averaged Navier Stokes models, where the particles are either treated as point masses (Eulerian-Lagrangian) or second continuum (Eulerian-Eulerian). Hence, various closures are required, such as considered particle forces as well as turbulence and rheology models.

[2] A constitutive equation is considered as a mathematical expression relating stress and strain and/or strain rates, or even other flow/material properties. A rheological model comprises a particular constitutive equations as well as certain assumptions made for a set of experimental data to fit material functions such as shear viscosity and first normal stress coefficient. However, in many cases these terms are used interchangeably.

data using a pipe viscometer [25]. Both real drilling fluids, which may show any combination of shear-thinning, yield stress, viscoelastic and thixotropic behavior, and model drilling fluids such as e.g. aqueous PAC solutions, may be used as experimental fluids. Preparing and mixing of constituent components is important for both real and model fluids.

Polyanionic cellulose (PAC) is a water-soluble biopolymer derived from Carboxymethyl Cellulose (CMC, E466) with a high degree of substitution (DS) of hydroxyl groups with sodium (NaCl), i.e. PAC is a high-quality sodium CMC with higher DS and thus molecular weight (MW) [26]. Like sodium CMC, PAC is produced from naturally occurring cellulose by etherification, where hydroxyl groups are substituted with sodium groups. The properties of the polymers, such as viscosity, molecular weight, etc., may be tailored by substitution of other functional groups into the chain. The DS determines the specific performance. As opposed to sodium CMC ($0.4 < DS < 0.8$ [26]), PAC features a $DS > 0.9$ [27] and features less residual sodium [28]. In drilling fluids, the main advantage of PAC compared to CMC is the better resistance to salt which provides improved shale inhibition characteristics as well as filtrate control [27]. The anions stabilize clay particles which improves filter cake texture and reduce risk of swelling of clay rich formations. However, salts do have a strong impact on the rheology of PAC and may even cause transition to Newtonian behavior [29].

For CMC solutions it is known that they are generally shear-thinning and viscoelastic [30,31] and feature thixotropic-like behavior [31–33]. They generally seem to obey the Cox-Merz rule [30]; however, as a consequence of restructuring processes they deviate from the Cox-Merz rule at high shear [34]. PAC solutions have so far been investigated much less. Given their relation to CMC, it is not surprising that they feature shear-thinning and viscoelastic properties [2].

The rheological information of aqueous PAC solutions used in cuttings transport studies [7–16] is usually disclosed in the form of model coefficients, such as the Ostwald/de Waele “Power law” model [21], and without any indication of the uncertainty of the measurements and model fit. PAC solutions in these studies are considered purely viscous, i.e. they are considered to feature neither viscoelastic nor time-dependent/shear-history dependent properties [7–15,17–19] and are thus modeled as GNF, most commonly employing a PL model. However, indication of viscoelastic [2,16] and time-dependent [19,29] behavior of PAC solutions exists, which is not surprising given the polymeric nature of PAC solutions.

This paper reports a complete rheological characterization of PAC solutions with regards to apparent viscosity, yield stress, time-dependent behavior, and viscoelastic properties, i.e. a comprehensive picture of the rheological properties. Characteristic time scales of the fluid (further referred to as ”rheological time scales”) are derived from the experimental data gathered. An estimate of the uncertainty associated with simplification of the physics of the fluid by assuming a purely shear-thinning rheology, i.e. treating it as a GNF, as usually done in numerical modelling of cuttings transport but also analysis of experimental data, is provided. We further provide an estimate of the uncertainty associated with the standard simplification of the physics of the fluid, assuming a purely shear-thinning GNF.

In section 2, we present the methodology and materials used to obtain the experimental data along with definitions of some of the rheological time scales later used in the interpretation of data. In section 3, the different rheometric test results are presented along with the derived time scales. Section 4 provides a discussion of the rheometric testing results as well as the corresponding time scales. Finally, in section 5, a conclusion and outlook is provided.

2 Materials & Methods

2.1 Equipment and general rheometric test protocol

Various rheometric tests were performed on different PAC solutions (generated with the same PAC granules) with two different rheometers:

- Flow curves (FC), with both controlled shear rate (CSR) and controlled shear stress (CSS).
- Amplitude sweeps (AS) with constant angular frequency as well as frequency sweeps (FS) with constant strain.
- 3 interval time tests (3ITT), with rotational-rotational-rotational (RRR) interval settings.

Figure 2 provides a timeline overview of this study's test protocol. The individual process steps (mixing, resting, rheometric measurements) will be presented in the following sections. To monitor phenomena such as natural degradation, fermentation, or off-gassing, additional flow curves were obtained regularly during the rheometric characterization at the times indicated in Figure 2 (0, 2, 5, 12, 48 h) with fresh samples from the prepared fluid stored in the glass jar. Due to equipment availability, different mixers and rheometers operated by different operating personnel were utilized, as depicted in Figure 2. The majority of the data was generated with the Waring LB20E*/Anton Paar MCR102 combination. Additional testing was conducted with the Silverson L4RT-A/Anton Paar MCR302 combination to supplement and cross-check the results.

The measuring systems utilized were concentric cylinders (CC27) with a gap size of 1.13 mm, conical bottom, and a nominal sample volume of 19.35 ml. The accuracy of the rheometers is specified with ±5% relative SD (SD_r) for a torque T > 5 nNm for rotation and T > 7.5 nNm for oscillation in case of the MCR102 and T > 1 nNm and T > 0.5 nNm in case of the MCR302, respectively. An accuracy of ±1% SD_r is specified for T > 10 µNm [35]. For the CC27 geometry utilized, the latter may be converted [36] to an apparent viscosity threshold given by

$$\eta_{\min} \approx 2.02 \cdot 10^{-1} \dot{\gamma}^{-1}. \tag{4}$$

In case of higher shear rates, i.e. rotation speeds, inertial instabilities such as Taylor vortices may develop. For the CC27 geometry utilized and a gap-dependent critical Taylor number of 1884 [37], the maximum apparent viscosity threshold to avoid Taylor vortices is then given by

$$\eta_{\max} \approx 8.389 \cdot 10^{-6} \dot{\gamma}. \tag{5}$$

2.2 Fluids

MI-Swaco Polypac R, as used in this study, is a white, odorless granulated powder with a molecular mass of 881.2 kDa (Mw). No treatment method, such as aging [38], was applied. Three different mixtures of MI-Swaco Polypac R and distilled water as summarized in Table 1 were used for all tests. The concentrations were chosen such that a typical drilling fluid apparent viscosity range [39] is covered. Most tests were done on PAC2 and PAC4, as these concentrations represent an apparent viscosity range resulting in transitional wellbore flows.

2.3 Sample preparation, resting and loading

Two different types of mixers as given in Figure 2 were used to mix the granular PAC with distilled water. The mixers were non-compliant with ISO 10416 [38] because they did not feature the required high-speed range. To obtain homogenously mixed samples for rheometric testing with the available mixers, the mixing procedures given in Table 2 were established and followed to prepare all samples.

The utilized rotational speeds of the different mixers during "Addition" and "Mixing" are a resulting best-working and mixer-dependent compromise of two contradictory requirements

- In order to keep the developing viscosity low and ensure homogenous mixing, the rotational speed has to be as high as possible.
- In order to entrain as little air as possible during mixing, the rotational speed has to be as low as possible.

After mixing, air bubbles were observed in all samples. However, in the case of the Waring LB20E*/ mixer, the observed bubbles were considerably smaller, probably due to the higher mixing speed utilized. After the resting periods, no air bubbles were observed in either sample.

The respective resting times were mainly due to laboratory availability constraints. However, a resting interval of 1 hour represents a realistic industrial time frame as applied by drilling service companies that perform on-site rheological measurements on drilling fluids on a daily basis.

The fluid samples were gently poured from the glass jar into the cylinder of the rheometers measuring system up to the marking line. The cylinder was inserted into its fixture on the rheometer and the measurement system/inner cylinder was lowered into the outer cylinder containing the sample. Measurements were not started until the rheometers indicated a steady temperature of 21°C.

2.4 Rheometer settings

The main rheometer settings of the different tests conducted in this study are summarized in Table 3. Temperature was controlled to T = 21°C by the rheometers in all cases. All measurements were conducted at ambient pressure. The reason is that typically cuttings transport studies are also conducted at ambient conditions and temperature scaling of polymeric solution is fairly well understood [31,32].

No pre-shearing was conducted in any of the tests summarized in Table 3. Standard pre-shearing definitions do not exist in the petroleum industry [38,40,41], other than that typically Fann measurements are conducted as a downward sweep, i.e. from high to low shear rates. Pre-shearing as used in various studies has been quite subjective, and has for instance been based on the high shear rates experienced at the drill bit. As the fluids resting time at the drill bit is very short, the relevance of such high pre-shear is not clear. Moreover, our overall objective is numerical cuttings transport modeling, where the computational domain is an annular subsection quite some distance from the bit. The influence of the high shear rate at the bit (applied to the fluid in a very short time only) is not expected to be of much relevance at an arbitrary wellbore element far from the bit. Finally, any other pre-shear would either be subjective or have to be based on the wall or average shear rate of annular flow, which is a function of fluid velocity, wellbore geometry, and flow exponent n, i.e. problem-specific. Thus, we decided for the following reproducible and unified approach: After gentle pouring of the sample into the measurement cylinder all samples where subject to a resting time (≈ 30 s … 1.5 min) until the rheometers temperature control reached the set point of T = 21°C. Note that for every rheometric measurement, a fresh sample from the glass jar was loaded into the rheometer and discharged after the measurement. Hence, every measurement was performed with a sample having a relatively comparable state of microstructure, since the shearing due to pouring should be equal for all the samples used.

2.5 Rheological time scales of the fluid

Various microscopic effects such as molecular motion (in the order of 10^{-15} seconds and therefore negligible) or structural changes may occur in a complex fluid. Consequently, there exists a corresponding variety of characteristic time scales for the respective relaxation times. Particular formulations of these fluid time scales often depend on the constitutive equations and/or material function used and may also depend on test data available. Since the degree of viscoelasticity and thixotropy is to be estimated, four rheological time scales are defined as follows [42]:

- The **GNF relaxation times $\boldsymbol{\lambda_{\mathrm{PL}}}$** and **$\boldsymbol{\lambda_{\mathrm{Cr}}}$**, which are based on the respective GNF material models, namely the Ostwald/de Waele “Power law” (PL) model [21] in its rearranged form, where the ordinary PL coefficient K_{PL} is expressed as $K_{\mathrm{PL}} = \eta_0 (\lambda_{\mathrm{PL}})^{(n_{\mathrm{PL}}-1)}$, which then yields

$$\eta(\dot{\gamma}) = \mu_0 \left(\lambda_{\mathrm{PL}} \dot{\gamma}\right)^{n_{\mathrm{PL}}-1} , \tag{6}$$

  and the Cross (Cr) [23] model

$$\eta(\dot{\gamma}) = \left(\mu_0 - \mu_\infty\right)\left(1 + \left(\lambda_{\mathrm{Cr}} \dot{\gamma}\right)^{n_{\mathrm{Cr}}-1}\right) + \mu_\infty . \tag{7}$$

  Note that the PL material function may be considered a special case of the Carreau [24] material function,

$$\eta(\dot{\gamma}) = (\mu_0 - \mu_\infty)\left[1 + (\lambda_{\mathrm{Ca}}\dot{\gamma})^2\right]^{\frac{n_{\mathrm{Ca}}-1}{2}} + \mu_\infty . \tag{8}$$

which approaches a PL material function for the case of higher shear rates and neglected infinite-shear viscosity μ_∞. Hence, the model coefficients in equation (6) may be considered equivalent to the coefficients and fit of a Carreau material function; however, they are not exactly identical.

- The **"Recoverable Shear"-based relaxation time λ_{RS}**, which is constructed from the GNF PL coefficients and coefficients of a PL fit of the First Normal Stress Difference (FNSD).

$$\lambda_{\mathrm{RS}} = \left(\frac{K_{\mathrm{FNSD}}}{2K_{\mathrm{PL}}}\right)^{\left(\frac{1}{n_{\mathrm{FNSD}} - n_{\mathrm{PL}}}\right)} \tag{9}$$

A PL material function does not capture the Newtonian viscosity plateaus at low and high shear rates. Therefore, PL coefficients are determined for a given point of the flow curve with the following conditions:

$$\eta_{\mathrm{PL}}(\dot{\gamma}) = \eta_{\mathrm{Cr}}(\dot{\gamma}), \qquad \frac{\partial \eta_{\mathrm{PL}}(\dot{\gamma})}{\partial \dot{\gamma}} = \frac{\partial \eta_{\mathrm{Cr}}(\dot{\gamma})}{\partial \dot{\gamma}} \tag{10}$$

- The **Maxwell relaxation time** λ_{Max} which is based on the linear viscoelastic Maxwell model, and consequently represents time scales on which the fluid acts in a linear viscoelastic manner.

$$\lambda_{\mathrm{Max}}(\omega) = \frac{G'(\omega)}{\omega G''(\omega)} \tag{11}$$

Experimental FS data may be used to estimate the order of magnitude of these time scales.

- The **3ITT relaxation time** $\lambda_{3\mathrm{ITT}}$, which is estimated based on time-dependent changes of the apparent viscosity due to instantaneous start-up/shut-down of a steady shear flow using 3ITT data. An exponential function of the form

$$\eta(t) = \eta_\infty + (\eta_0 - \eta_\infty)\, e^{-\frac{1}{\lambda_{3\mathrm{ITT}}}t} \tag{12}$$

is used for this purpose, with the rheological relaxation time $\lambda_{3\mathrm{ITT}}$ being the corresponding time constant it takes to relax to 63% to the dynamic equilibrium value.

3 Results

3.1 Flow Curves

A Flow Curve (FC) is considered to represent the equilibrium apparent shear viscosity of a fluid sample over a range of relevant shear rates. Figure 3 depicts the obtained FCs for all PAC concentrations. The apparent viscosity indicated is the mean of 13 (PAC4) and three (PAC2, PAC8) measurements. Additionally, data obtained from the literature is displayed using unfilled symbols. For all concentrations tested with a constant MPD of Δt = 5 s, a prominent hysteresis effect was found. Figure 3 shows two solid lines for each PAC solution, representing means of the upward (higher curve) and downward (lower curve) sweep respectively, the mean of these two means is represented by the solid line. The FC obtained with a logarithmically decreasing MPD of Δt = 120…2 s log (here depicted with a thick dashed line) shows almost no hysteresis effect and thus may be considered the equilibrium FC [43]. Most of the FC data sets from the literature do not show any hysteresis effect. However, the data of Johnsen (2014) [13] and [18] (not displayed) also indicate a small hysteresis effect for intermediate shear rates.

Additionally, in the case of PAC4, the natural scatter of the whole measurement process was identified through measurements of 13 FC (Not depicted in Figure 3). Each FC was obtained with a fresh sample from the prepared mixtures. Arithmetic mean and standard deviation (SD) were established for both upward and downward sweeps separately. For PAC4, the obtained mean ±3·SD of upward/downward sweeps are respectively indicated in Figure 3 by dotted lines.

All results indicate a constant Newtonian viscosity at low shear rates for all tested concentrations. FCs obtained with a constant MPD of Δt = 5 s show a large variance of data at very low shear rates, as indicated by the diverging dotted lines in Figure 3. Most of the FC data sets from the literature do not cover the low shear rate range ($\dot{\gamma}$ = 0.01…1 s^{-1}). However, Time et al. (2015) [19] and Khatibi et al. (2016) [29] have covered the shear rate range $\dot{\gamma}$ = 0.1…1 s^{-1} and the respective data sets also do indicate a Newtonian viscosity plateau in the low shear rate range.

The different data sets plotted in Figure 3 are not coinciding for a particular fluid concentration. However, in case of PAC4, most datasets are fully enclosed by the arithmetic mean ±3·SD boundaries of our data. The five FC obtained in order to monitor natural degradation (as described in Figure 2, not displayed in Figure 3), are within arithmetic mean ±3·SD boundaries. No time-dependency, e.g. a change of an apparent viscosity at a certain shear rate with time, was observed over the duration of the experimental campaign.

Fitting the PL, Carreau and Cross material functions (6)-(8) to the equilibrium FCs yields model coefficients as summarized in Table 4.

3.2 Amplitude Sweeps

Amplitude sweeps (AS) provide the dependence of the loss modulus G'' (characterizing the viscous property of a material sample) and storage modulus G' (characterizing the elastic property of a material sample) over a range of relevant strain for a given frequency of oscillatory motion and thus allow for quantification of the viscoelasticity of a material. Results for PAC4 and PAC2 are depicted in Figure 4.

The loss modulus G'' exceeds the storage modulus G' for the entire strain range tested. While for the lower strain range, e.g. γ < 10%, G' and G'' do have the same order of magnitude, G' and G'' differ by more than one order of magnitude for the higher strain range, e.g. γ > 500%. The phase shift angle ϕ, defined as

$$\phi = \arctan\frac{G''}{G'} \ , \tag{13}$$

is an indication of ideal solid behavior for 0° and ideal fluid behavior for 90°. In case of the investigated PAC4 sample, the phase shift angle ϕ ranges from 66° to 70° for strains smaller than 1% and reaches 86° at a strain of 1000% (corresponding to a shear rate of $\dot{\gamma}$ = 100 s^{-1} for the set angular frequency of ω = 10 rad/s). The PAC2 phase shift angle exceeds the PAC4 phase shift angle for the entire strain range investigated.

3.3 Frequency Sweeps

As opposed to AS, frequency sweeps (FS) provide the dependence of the storage modulus G' and the loss modulus G'' over a range of relevant oscillation frequencies for a given amplitude of strain. Results of PAC2 and PAC4 FS are depicted in Figure 5. In the low angular frequency range (ω = 0.1…10 rad/s), G' is smaller than G' by almost one order of magnitude. Towards the high angular frequency range, the G' increases more than G''. Between ω = 20 rad/s and ω = 30 rad/s, the G'' equals the G' for the PAC2 data, and at ω = 20 rad/s for the PAC4 data. Based on Eq. (11), the upper Maxwell time scale representing viscoelastic effects is estimated as $\lambda_{\mathrm{Max}}(\omega = 0.1\ \mathrm{s}^{-1}) \approx 0.67$ s for PAC4.

3.4 Three Interval Thixotropy Tests

Three Interval Thixotropy Tests (3ITT) were conducted with PAC2 and PAC4 in order to establish the time-dependent behavior of apparent viscosity due to microstructural changes. Figure 6 shows 3ITT-RRR (→ RRR: Three intervals of rotational shear) results for a 100-50-500 s interval definition and Figure 7 for 300-600-500 s, where the length of the third interval was limited by laboratory availability constraints.

Apparent viscosity is plotted as a function of time as a response to the step-like changes of the imposed shear rate. The PAC2 data was partly smoothed with a time average filter because it featured quite scatter, presumably due to the much lower apparent viscosity level. In all cases, the apparent viscosity follows the step change from the very low to the very high shear rate instantly. However, after the intermediate high shear-rate interval, the apparent viscosity shows a remarkable time-dependent recovery in the third interval. In the case of the 100-50-500 s intervals (Figure 6), the apparent viscosity overshoots the reference level, almost instantly for PAC 2 and exponentially for PAC4. In both cases, a second relaxation phase follows the overshoots in which the apparent viscosity develops almost back to the reference level. In the case of the 300-600-500 s intervals (Figure 7), the apparent viscosity undershoots the reference level, almost instantly for PAC 2 and exponentially for PAC4. Again, the apparent viscosity develops further and gradually increases to almost the reference value of the first interval towards the end of the experiment.

For the immediate response to the step from high to low shear rate, the rheological relaxation times λ_{3ITT}[3], estimated based on curve fitting of Eq. (12) to the experimental data and depicted in black in Figure 6 and Figure 7, are in the order of 10^1 s for the initial response of PAC 4. Zooming in to the very few seconds after the step (red subplot in Figure 7), reveals a time scale in the order of 1 s for PAC2.

The second relaxation phase features much larger time scales in the order of several 10^1 s for PAC2 (Figure 7) to several 10^2 s for PAC4, as depicted in Figure 8, where the PAC4 3ITT data is normalized with the corresponding FC apparent viscosities. Fitting the growth function, i.e. Eq. (12), to the more gentle increasing part of the third interval provides a time scale of 392 s for the 300-500-300 test and 126 s for the 100-50-500 test.

The intermediate, i.e. high shear rate intervals do apparently show time-dependent apparent viscosity as well. Using a decay function, similar to Eq. (12) but with η_0 and η_∞ exchanged, reveals the time constant for the second high shear rate interval of the 300-600-500 s interval case to be in the order of 615 s.

In addition, Figure 8 provides a clearer picture of the first interval, the purpose of which is to establish an equilibrium reference level. The apparent viscosity readings are not stable and equal to the equilibrium FC values. Assuming that the time scale identified in the third interval is the relevant one for the low-shear situation of the first and third interval, one may conclude that the first interval needs to have a duration of approximately 1200 s ($3 \cdot \lambda_{3\mathrm{ITT}}$) in order to yield stable reference values for any initial state of the samples microstructure.

3.5 Normal stresses & Cox-Merz empirism

Since we are only interested in order of magnitude estimates, we did not directly measure normal stresses but rather exploited the FS results, namely the complex viscosity η^* as a function of the angular

[3] The rheological relaxation time $\lambda_{3\mathrm{ITT}}$ may alternatively be defined as the time it takes to fully relax to an equilibrium state. Here, the definition of a time constant is used as described in Eq. (9). The applied definition of $\lambda_{3\mathrm{ITT}}$ therefore represents the time it takes to relax to ≈ 63% of its final value.

frequency ω, and estimated the first normal stress differences (FNSD) N_1 based on the first normal stress coefficient (FNSC) Ψ_1 using Laun's rule [44]

$$\Psi_1\left(\dot{\gamma}\right) = 2\frac{G'}{\omega^2}\left(1+\left(\frac{G'}{G''}\right)^2\right)^{0.7}\Bigg|_{\dot{\gamma}=\omega} \tag{14}$$

Figure 9 shows the estimated FNSC Ψ_1 for the case of PAC2 and PAC4 as well as the corresponding time scale estimates λ_{RS} as defined in Eq. (9), where the PL coefficients are determined point-wise to more closely follow the apparent viscosity function using the conditions (10). Additionally, the Cross fit of the apparent viscosity as provided in Table 4 and the complex viscosity η^* are depicted. The complex viscosity η^* is plotted over the shear rate utilizing the Cox-Merz rule [45]. The time scale estimate λ_{RS} is in the order of $5 \cdot 10^{-2}$ s for PAC2 and $2 \cdot 10^{-2}$ s for PAC4.

The relevance of normal stresses and thus viscoelasticity may be judged by comparing it to the shear stress for a given shear rate. Figure 10 depicts the shear stress τ based on the Cross fit of the apparent viscosity as given in Table 4, the estimated FNSD $N_1 = \Psi_1 \cdot \dot{\gamma}^2$ as well as the recoverable shear $N_1/2\tau$. The recoverable shear exceeds a value of 0.5 for shear rates larger than approximately 13 s^{-1} (PAC2) and 25 s^{-1} (PAC4).

4 Discussion

4.1 Range of time scales

The obtained rheological time scales for PAC2 and PAC4 are summarized in Figure 11.

Two groups may be distinguished: The 3ITT time constants have the order of magnitude $10^1 \ldots 8 \cdot 10^2$, the GNF time constants, the Maxwell relaxation time and the FNSD time constant have the orders of magnitude $10^{-3} \ldots 1$. Since the Maxwell as well as the RS time scales are characteristic for the viscoelastic behavior of the PAC solutions, we attribute these time scales range to viscoelasticity. With the same reasoning, we attribute the 3ITT time scale range to microstructural changes of the PAC solution as a consequence of accumulated shear, i.e. thixotropy. This distinction is important if one wants to design constitutive equations accounting for both the viscoelastic and thixotropic features [46].

While the RS time scales certainly indicate the correct order of magnitude, its numerical values are not correct over the entire range of shear rate. As may be seen from Figure 10, the simple FNSD fit does not accurately capture the lower shear rate range.

4.2 Shear-thinning behavior

4.2.1 Transient effects at low shear rates

The FC data indicates a transient behavior of the fluid samples at very low shear rates resulting in large uncertainty ranges of the apparent viscosity (Figure 3). As the equilibrium PAC4 FC data demonstrates, a MPD of Δt = 120…2 s log (or longer) is much better suited than a constant value of 5 s to allow for an equilibrium fluid microstructure at very low shear rates. This is confirmed by the 3ITT results, where a preliminary quasi-equilibrium is reached only after approximately 30 s ≈ $3 \cdot \lambda_{3\mathrm{ITT}}$ (Figure 7) for the investigated shear rate step. For the very low shear rate range $\dot{\gamma} = 10^{-2} \ldots 10^{-1}$ s^{-1}, a MPD of Δt = 120…2 s log yields a total strain of γ = 1.2…6 as opposed to γ = 0.05…0.5 for the MPD Δt = 5 s, i.e. the logarithmic MPD used leads to much more strain and thus microstructural equilibrium. In general, a strain of γ = 5 is considered a minimum to ensure microstructural equilibration [47].

4.2.2 Hysteresis

The FCs obtained with a constant MPD consistently feature a hysteretic area indicating thixotropic [48], or more general, time/shear-history-dependent behavior. Most of the benchmarked data obtained from the literature do not show a hysteresis loop. In the case of PAC4, the logarithmic MPD and Johnsen (2014) [13] data show a much smaller degree of hysteresis in some parts of the investigated shear-rate range. Primarily, this may also be attributed to MPD settings, as described in 4.2.1. Since FCs are considered to refer to the equilibrium behavior of the fluid, a full equilibrium of the loaded sample needs to be established prior to sampling the apparent viscosity.

Another important factor is the total time of shear, which varies greatly between the two MPD concepts. For instance, in the case of the constant MPD of Δt = 5 s, the total time of shear is about 150 s at $\dot{\gamma}$ = 16.1 s^{-1} (upward sweep). In the case of the logarithmically decreasing MPD of Δt = 120…2 s, the corresponding total time of shear is about 663 s, which may allow for a better dynamic equilibrium of the fluid microstructure and consequently an apparent viscosity value consistent with the upward sweep.

4.2.3 Scatter of different flow curves

The SD for most of the shear rate range tested is in the order of the specified accuracy of the rheometer. When expressed as SE, the order of magnitude is consistent with the typical experimental error of 1-10% for rotational rheometry [49]. The FC obtained from the literature coincide neither with each other nor with our logarithmic MPD data. The spread is consistent with technical work performed [50] to develop ISO 13500 [51], where intra-lab differences, when obtaining FC of PAC according to ISO 10416 [38], are estimated to be less than 10% SD; however, using Fann viscometers.

With reference to the elements of Figure 1, intra-lab differences may arise due to various rheometric characterization process parameters, which may differ between studies and laboratories:

- **Rheometer**

    - Type of rheometer
    - Measurement point duration (MPD), see 4.2.2
    - (True) sample temperature [49]
    - Measuring systems (Concentric Cylinder, Cone & Plate)
    - Natural scatter of measurement process/accuracy
- **Preparation & mixing**
    - Type of mixer
    - Geometry of mixers utilized, e.g. blade vs. jug geometry/size
    - Mixing speed and duration
    - Resting time
    - Sample volume
    - Effect of air bubbles
    - Sample transfer
    - Impurities, e.g. unclean equipment, usage of non-distilled water with an effect on pH

The total difference of one FC to another is the sum of all the possible differences of above mentioned process parameters. In case of our data, the observed test data differences may be most likely attributed to the different MPDs (see 4.2.2), but possibly also because of the different mixer types, and resting times utilized.

The effective shear rate and the total strain of the mixing process are a function of the mixer geometry, mixer speed and the total mixing times. The two mixing processes differ regarding the average shear rate, which is higher for the Waring LB20E*/ case by a factor of 1.65, regardless of whether estimated with the ratio of circumferential velocity/blade radius or impeller rotational speed times impeller geometry constant. Furthermore, the degree of turbulence generated during the mixing process is substantially higher for the Waring LB20E*/ mixer with a mixer impeller Reynolds number of the order Re_{Imp} ≈ 4650…11627 vs $\mathrm{Re}_{\mathrm{Imp}}$ ≈ 600…1500 for the Silverson L4RT-A. Finally, cavitation may have occurred in the case of the Waring LB20E*/ (Cavitation number ≈ 1.5) as opposed to the Silverson L4RT-A (Cavitation number ≈ 20). Hence, the overall mixing quality of the Waring LB20E*/ seems to be much different from the the Silverson L4RT-A. Possibly the higher degree of shear, turbulence and inception of cavitation might have altered the polymeric microstructure and affected the measurements.

The nominal resting times applied in the two preparation processes were very different (1 h vs. 48 h). This may have allowed to further develop a higher-quality solution in the case of the 48 h samples, as diffusion processes may have further dissolved remaining granules and completely hydrated the polymer. In addition, more and smaller air bubbles (which were more likely to occur in the case of the Waring LB20E*/ due to the higher degree of shear and turbulence) may have left the system. For a time frame of one hour (Waring LB20E*/), the cut-off size for bubbles that would have degassed from the bottom of the jar to the top (liquid height ≈ 0.1 m) is d_p = 0.1 mm, whereas d_p = 0.0146 mm for a time frame of 48 h (Silverson L4RT-A)[4].

However, the effective resting times in case of the Waring LB20E*/ fluid samples were substantially longer for most of the samples, as the prepared fluid was further left to rest in the sealed glass jars until the actual sample for the individual measurement was taken. No significant differences (with respect to the established SDs) were observed in the subsequent FC measurements at the times indicated in Figure 2, indicating that the discussed MPD settings is the primary influence on the different FC.

4.2.4 Newtonian plateau at low and high shear rates

PAC solutions feature a Newtonian viscosity plateau at low shear rates, as one would expect because of their polymeric nature. This low shear-rate Newtonian viscosity plateau requires the application of an appropriate viscosity model such as the Cross [23] and Carreau [24] family of models if one is interested in that shear-rate range, e.g. the settling of particles in drilling fluids, and a GNF rheology model is assumed to adequately describe the FC data.

The same applies if one is interested in higher shear rate ranges, as the PAC solutions investigated feature a corresponding Newtonian plateau, which, in the absence of data available, may be taken equivalent to the solvent viscosity. However, precise high-shear rate data becomes important to not underestimate the laminar shear viscosity of the fluid, as it would occur using a PL material function [53].

[4] Based on zero shear rate viscosity μ_0 of the system and Schiller-Naumann [52] drag law.

In the context of CFD modelling, where a rheological model is required as input (Figure 1), it is also very beneficial for the computational process if a four-parameter material function of the Cross [23] and Carreau [24] family of models is used, as some control volumes in the domain will always feature low shear rates and, during the iteration process, some other might see shear rates much higher than the final value. This may increase numerical stability because iterations are based on fitted rather than extrapolated rheometric data or cut-off values. Furthermore, regions of low shear are ubiquitous in every flow problem. In addition, the high shear rate region above the range of interest is important when it comes to turbulent flow modeling in order to avoid extrapolation errors of the laminar shear viscosity [53].

In addition, for higher shear rate ranges, extensional viscosity effects may lead to turbulent drag reduction (DR) because of stretching of polymer molecule chains. This is well understood for CMC, where comparable concentrations may lead to DR of 10 - 35% [54]. If relevant, one may account for DR by appropriate models, e.g. [55].

4.3 Viscoelastic behavior

4.3.1 Relevance of elastic properties

The investigated PAC solutions exhibited relevant viscoelastic properties for very low strains (Figure 4) or high frequencies (Figure *5*), since both loss and storage modulus were of the same order of magnitude. However, elasticity seems negligible for continuous deformation, i.e. strains larger than 1000%, since the phase shift angle ϕ at a strain of 1000% has a value of 82.5° for PAC4 and 86° for PAC2, with a phase shift angle ϕ = 90° representing purely viscous behavior. In that sense, PAC2 is less viscoelastic because the phase shift angle is exceeding the one of PAC4 over the entire range of strain, i.e. for a given strain PAC2 is more fluid-like than PAC4. Hence, PAC4 represents a worst-case in terms of viscoelasticity.

If continuous deformation, i.e. flow over a sufficient amount of time and therefore large strain, takes place, the elastic response of the microstructure seems negligible. This is the case in a steady-state drilling operation; hence, PAC solutions used to investigate such operations may be treated as purely viscous. However, in regions of low deformation, for instance the interstitial drilling fluid in a cuttings bed, viscoelasticity may not be negligible.

On the other hand, normal stresses, which are caused by strain-induced microscopic anisotropy where polymer molecules depart from their equilibrium shape, become more relevant at higher shear rates, as depicted in Figure 10. The recoverable shear $N_1/(2\tau)$ is usually considered as a degree of elasticity, where a value of larger than ½ indicates high elastic behavior [56]. The effect of normal stresses on particle settling is well-known and may have to be accounted for in case of high settling shear rates using the estimated viscoelastic time scales provided in Figure 11 and an appropriate model, e.g. [57].

The estimated viscoelastic time scale range λ_{Max} is only valid for small deformations as it is based on the Maxwell model. The Maxwell model does not describe the data completely as the slopes of both G' and G'' in the FS are not equal to 2 and 1 respectively [48]. However, comparing the FC apparent viscosity with the results from the FS by utilizing the Cox-Merz rule (Figure 9), we find that the two curves do reasonably well coincide for the lower shear rate range, i.e. the Maxwell-based time scales may serve as a first approximation. However, like CMC solutions [34], PAC solutions deviate from the Cox-Merz-empiricism for higher shear rates as a consequence of the internal restructuring processes.

Viscoelasticity is relevant on short timescales. This is also apparent from Figure 8, where viscosity and corresponding stress overshoots are observable just after the shear rate step from interval two to three. These overshoots do have a quite large amplitude; hence, on these short time scales, elastic effects are both present and significant quantitatively.

4.3.2 Yield stress

No yield stress is evident for the strain range investigated since the loss modulus G'' always exceeds the storage modulus G' and no crossing of the two moduli occurs (Figure 4). In addition, the CSS FC tests (not depicted) did not show any evidence of yielding.

This may seem conflicting with other studies stating that PAC increases the yield point/yield stress in drilling fluids [1,3,5,6] or, more generally, that anionic surfactants affect the yield stress of Bentonite slurries [58]. However, as opposed to this study, where purely PAC in an aqueous solution is used to

create a model drilling fluid, the above cited studies actually investigated drilling fluid systems, where PAC is one of multiple additives to e.g. Bentonite-based suspensions. Here, the PAC anions may stabilize the clay particles and thus stabilize the suspension and indeed increase an existing yield stress. In addition, as per drilling industry convention, all these studies have applied either the HB or the Bingham [20] material function to their data, which were obtained with Fann viscometers. Thus, yield point/yield stress as employed in these studies and defined in the drilling industry [40] is to some extent a model artefact rather than a feature of the obtained rheometric data since it is purely based on the two conventionally taken data points at Fann viscometer speeds θ_{300} and θ_{600} (Bingham model) or θ_3 and θ_6 (Herschel-Bulkley model) [40]. A more firm (but also more time-consuming and complex) approach may be taken by adopting a material function which better describes the data, e.g. HB instead of Bingham, and by determining a yield stress based on e.g. crossover points in the AS test or performing shear stress sweeps in a CSS mode and plotting stress vs. strain [59].

For higher concentrations or smaller strains than the ones investigated in this study, i.e. 8 g/L, a yield stress may develop in pure PAC solutions. However, for higher polymer concentrations, the resulting increase in apparent viscosities disqualifies such high concentrations for use as they are exceeding the typical range of drilling fluid viscosities [39].

4.4 Time-dependent behavior

The tested PAC fluids generally show time-dependent, or more precisely shear-history dependent behavior. After the step from low to high shear rates, stress/viscosity jumps almost instantly to a new preliminary equilibrium value; however, followed by a transient behavior of stress/viscosity with large rheological relaxation times in the order of 10^3 s. From high to low shear rates, transient behavior and relaxation are observed with a rheological relaxation time in the order of 10^0 s (PAC2) and 10^1 s (PAC4), with a second subsequent transient behavior of stress/viscosity with large rheological relaxation times in the order of 10^2 s (PAC2) and 10^3 s (PAC4). The observed dynamics are not a result of the change of the flow field (high to low shear rate step and subsequent change of the velocity field) as the time scale associated with the change of the velocity field is in the order of $<10^{-2}$ seconds[5].

The general change of apparent viscosity with time in the second and third 3ITT intervals confirms the time-dependent behavior of the investigated PAC fluids, as indicated by the hysteretic flow curves. Physically, this may be attributed to the interaction of the long-chain PAC molecules and the break-down/development of a three-dimensional structure in the solution. The high deformational load in the second interval will cause the polymer chains to align with the shear forces, resulting in a decreasing viscosity. In the transition to the recovery interval, the high load may have initiated a spontaneous rearrangement or crystallization of the polymer chains, which may further entangle over time, leading to an increase in viscosity. This may already be observed in the reference values of the 3ITT, where a transient behavior of the sample is visible indicating time-dependent behavior of the apparent viscosity. An even longer first interval, i.e. a sufficient amount of strain as described in 4.2.1, is required to get rid of all dynamics in the sample and reach dynamic equilibrium, i.e. stable reference values.

A large scatter of the amplitude of viscosity occurs in the third interval of the 3ITT. We consider this a consequence of the apparent viscosity levels (in particular regarding PAC2) as well as a MPD setting issue since the MPD in the third test interval is just 0.5 s, whereas the MPD in the first interval is 5 s and thus acting as a time filter.

Strikingly, PAC2 shows more pronounced over- and undershoots than PAC4, even though it can build less microstructure due to its lower concentration. Within this study, the described time-dependent behavior has been observed for two different concentrations as well as two shear rate steps only. A more comprehensive test matrix combined with much longer time intervals seems required and thus further work is needed to investigate the time-dependency of PAC solutions.

---

[5] This estimate may be obtained by rearranging the momentum balance for pure shear flow in the rheometer gap and inserting the two extremes of apparent viscosity η = 0.0275 Pa·s and η = 0.2 Pa·s, the density ρ = 999 kg/m³ and the rheometer gap size y = 1.013 mm.

$$\frac{\partial u}{\partial t} = \frac{\eta}{\rho}\frac{\partial^2 u}{\partial y^2} \quad \rightarrow \quad \delta t \approx \frac{\rho y^2}{\eta} \qquad \textbf{Error! Main Document Only.}(14)$$

The inverse of the RHS yields the corresponding time scales $\delta t(\eta$ = 0.0275 Pa·s) = 0.046 s and $\delta t(\eta$ = 0.2 Pa·s) = 0.0064 s for the change in velocity δu as a result of the change in shear rate $\delta\dot{\gamma}$.

4.4.1 Long-term behavior

Within the time frames of our experiments, we could not observe a full structural recovery of the viscosity under- and overshoots. Viscosity overshoots have also been observed with oil-based drilling fluids; however, these fluids may fully relax to the reference value after sufficient time [59]. This is also observed in the case of the 100-50-500 3ITT data, where the apparent viscosity eventually relaxes back to the reference value (Figure 8). However, this relaxation takes place on even larger time scales than the ones describing the initial transient response given in Figure 7.

The large time scales identified in the 3ITT tests ($\lambda_{3\mathrm{ITT}} \approx 391 \ldots 615$ s) indicate that even the FC obtained with a logarithmically MPD is not yet fully representing the dynamic equilibrium: For small shear rates such as $\dot{\gamma} = 0.1$ s^{-1}, the apparent viscosity changes by ≈ 8% with $\lambda_{3\mathrm{ITT}} = 391$ s (Third interval, Figure 8) and for large shear rates such as $\dot{\gamma} = 1200$ s^{-1}, the apparent viscosity changes by ≈ 5% with $\lambda_{3\mathrm{ITT}} \approx 615$ s (Second interval, Figure 8). These time scales also show that the sample's resting time in the measurement device could have been longer in order to ensure better structural reformation after the pouring process.

4.4.2 Thixotropic vs. time-dependent behavior

The fluid samples behavior is of classic thixotropic nature because as the change in viscosity is fully reversible, which is associated with a microstructure breakdown and complete reformation [48]. However, the observation of complete structural reformation depends on the time frame of the experiment. If the time scale of observation is chosen to be shorter, for instance in the order of the initial transient response (Figure 7), the reformation process is still occurring and the apparent viscosity difference is in the order of 10%.

4.4.3 Simplification to viscous behaviors

We have shown that PAC solutions generally feature time-dependent behavior. For small deformations and/or high frequencies, a linear viscoelastic behavior is evident; for high shear rates normal stresses differences may become important. Furthermore, PAC solutions show thixotropic behavior on larger time scales, with a nonlinear increase of the time scale as a function of the concentration.

In principle, a simplified treatment of the investigated PAC solutions as GNF is to be justified with respect to the actual flow problem as it depends on the ratio of i) the elastic or microstructural rheological time scales and ii) the characteristic process time scales and the time of observation in a Deborah number sense [60].

For very short process time scales, elastic effects are relevant, especially as they apparently may result in large amplitudes.

For longer process time scales, the thixotropic microstructural effects become relevant. However, here the corresponding amplitude ratios are much less pronounced, as may be verified both from the FC hysteresis (Figure 3) and normalized 3ITT apparent viscosity plots (Figure 8). For the PAC4 hysteresis, the downward sweep mean apparent viscosity at an intermediate shear rate is 83 - 90% of the upward sweep mean apparent viscosity. For the PAC4 3ITT relaxation, the apparent viscosity values reach 95% of the reference value in $2 \cdot \lambda_{3\mathrm{ITT}}$ by definition and for the PAC4 examples given in Figure 7, the apparent viscosity has reached approximately 80% of the final value in $\Delta t = 5$ to 7 s, which corresponds well with the apparent viscosity ratio of the FC downward and upward sweep given above.

For a PAC4 flow problem where the relevant time scale is in the order of the MPD $\Delta t = 5$ s, e.g. particles falling out of suspension and settling to the lower part of a horizontal wellbore section, the hysteretic FC presented in Figure 3 may be used to estimate the increase of uncertainty if the observed hysteretic loop, i.e. the change in time-dependent apparent viscosity due to change of the microstructure, is neglected. For modeling purposes, one may represent this hysteretic FC with the mean of the upward and downward sweep means, i.e. the dotted line in Figure 3 plus/minus a respective tolerance. For the given example, these tolerances may be estimated from the extremes as a result of natural scatter (Dotted lines of PAC4 FC in Figure 3). Thus, instead of having one FC, which may be used to fit a material function, one now has a FC with an increased uncertainty accounting for time-dependent effects.

For the given FC example, the relative standard uncertainty of both the upward and downward sweep is in the order of ≈ ±5% for $\dot{\gamma} > 140$ s^{-1} and ≈ ±10% for $\dot{\gamma} < 30$ s^{-1} (based on respective means (solid

lines) depicted in Figure 3 ±3·SD)[6]. If the hysteresis loop is neglected, the dashed lines are taken as ±3·SD and hence the uncertainty for this mean of the upward and downward sweep mean (dotted line) increases to ≈ ±15% for $\dot{\gamma}$ < 30 s^{-1} and ≈ ±18% for $\dot{\gamma}$ < 5 s^{-1}, which is a relative increase of 75 to 90%. The uncertainty of the range $\dot{\gamma}$ > 140 s^{-1} remains the same and for shear rates $\dot{\gamma}$ < 0.3 s^{-1} there is no reliable uncertainty estimate possible as the MPD effect (see 4.2.1) overshadows and thus increases the hysteretic loop uncertainty intervals. In addition, the 3·SD interval is approximately equal to the range of scatter representing intra-lab differences. Figure 3 shows that the uncertainty estimate (dashed lines) encloses the PAC4 results obtained from the literature as well as the assumed equilibrium FC. Thus, for the case of MPD Δt = 5 s, intra-lab differences (which may be due to one or a combination of the factors given in 4.2.3) lead to an apparently equivalent uncertainty magnitude as time-dependent effects.

It is important to note that this uncertainty estimate additionally includes the natural scatter of the FC measurement process as well as discussed factors such as MPD, mixing process and resting times as it is based on 3SD of both the upward and downward sweeps.

Note also that the order of magnitude of the FC hysteresis is dependent on the MPD, i.e. the time scale of observation, as well as the shear rate step. The latter is small for a FC sweep, in case of larger shear rate gradients the above given uncertainty range may underestimate the apparent viscosity. Hence, performing 3ITT tests for different shear rate steps will provide a better understanding of how uncertainty scales with shear rate steps and the time scale of observation.

However, a better approach for modeling activities obviously is to use the equilibrium FC instead of averaging the hysteretic FC. This imposes a constraint on experimental modeling in order to minimize the uncertainty when it comes to validation as indicated in Figure 1. Proper dynamic equilibrium i.e. a constant apparent viscosity needs to be ensured prior to sampling the variables of interest. Given the largest time scales identified ($\lambda_{3\mathrm{ITT}}$ = 615 s), this may not be practically possible as it yields very long laboratory times.

Finally, with respect to CFD modeling, the total uncertainty associated with a rheological model utilized is the root sum of the squares of individual uncertainties of every process step required to construct the rheological model. With reference to Figure 1, the fluid may feature more complex physics, which if neglected, increase uncertainty by potentially 75 to 90% as described above. The preparation process may increase uncertainty due to the various reasons mentioned in 4.2.3, in particular mixing procedures and resting times. The measurement process as such provides scattered data with a certain SD, here ±1% to ±5%, and is sensitive to the measurement settings (4.2.1, 4.2.2). Uncertainty will further increase (at least for certain ranges of shear rate) if an inappropriate material function is selected to represent the data as discussed in 4.2.4 and 4.3.2. The fit of the material function to the rheometric data by regression may further increase uncertainty (Table 4).

4.5 Substitution of drilling fluids in laboratory studies

In general, the investigated PAC solutions seem capable of serving as model systems for drilling fluids in laboratory cuttings transport studies (referring to “Test fluid” in Figure 1) since they feature shear-thinning behavior, and also show viscoelastic and thixotropic behavior.

The identified large thixotropic time scales ($\lambda_{3\mathrm{ITT}}$ ≈ 10^2…10^3 s) do have the same order of magnitude as water-based drilling fluids (WBDF) such as bentonite [43,61] and KCl [61] dispersions, as well as oil-based drilling fluids (OBDF) [59]. Moreover, the relative change in amplitude is also comparable to the behavior of WBDF [43,61] and OBDF [59]. However, as opposed to bentonite-based WBDF, the investigated PAC solutions do show a much smaller thixotropic time scale ($\lambda_{3\mathrm{ITT}}$ ≈ 10 s) for the first part of the microstructure build-up after stress relieve [43].PAC solutions do not show a yield stress for the concentrations investigated. Regardless of how to define and measure a yield stress, a yield stress is assumed a desirable property of a drilling fluid, keeping particles in suspensions at zero flow. The addition of Xanthan gum may be one way to develop a yield stress and keeping translucency as it is known to add viscoelasticity (but may also further increase shear thinning) [62].

Another important parameter to consider is density, which is basically equal to water for the investigated PAC solutions. The variations in relative fluid density between drilling fluids and rock may vary with a

[6] Usually, standard uncertainty is based on SD. Here, we base it on 3·SD as this encompasses 99% of the scattered data and is consistent with Figure 3.

factor of 1 to 3 [39]. However, relative density effects are well understood and there is no need to match relative density in experiments[7] as long as the variation is smaller than one order of magnitude. It is more important to match the sedimentation velocities of cuttings which may be controlled by the particle size.

[7] Besides scaling the problem, addition of Laponite may be considered in order to increase density and further develop time-dependent behavior [63] by keeping the required translucency [64].

5 Conclusions

Aqueous PAC solutions apparently feature linear viscoelastic properties in case of low strains and/or high frequencies and exhibit relevant normal stress differences in case of high shear rates, but no yield stress. They further show time-dependent, or more precisely shear-history dependent behavior.

When performing flow curve measurements, sufficiently long measurement point durations over the entire range of shear rates are required to obtain a microstructural equilibrium in the sample. This is critical in order to minimize the uncertainty due to thixotropic effects and to obtain the most reliable fit to applied rheological models.

For cuttings transport modeling purposes, it seems reasonable to treat PAC solutions as purely viscous, shear-thinning, fluids as long as

- small deformations and/or large frequencies as well as higher shear rates are not relevant for the problem; hence, neglecting elastic properties.
- the time of observation is sufficiently longer than the fluids rheological relaxation times, i.e. that an equilibrium of the problem with respect to the fluids flow field and microstructure is achieved; hence, time-dependent restructuring effects are becoming irrelevant.

If this is not satisfied, the overall uncertainty of the rheometric flow curve data, i.e. sum of the general experimental uncertainty and an additional uncertainty associated with the purely viscous interpretation of the data and corresponding model coefficients, may increase by an order of ≈ 75 to 90%. Further work is required to detail this estimate with regards to the time scale of observation as well as shear rate steps and relate it to specific cutting transport process time scales.

Instead of a yield stress, pure PAC solutions feature a low-shear viscosity plateau and require a corresponding material function, e.g. Cross/Carreau, if the low shear rate range ($\dot{\gamma} < 1\ s^{-1}$) is relevant for the particular problem investigated. For modeling purposes, the application of a Cross/Carreau material function is beneficial because it minimizes the negative effects of extrapolation of the conventionally used Power Law material function.

Acknowledgements

The project Advanced Wellbore transport Modeling (AdWell) with its sponsor, PETROMAKS 2/the Research Council of Norway (project 228391) and its partners Statoil, Neptune Energy Norge AS, IRIS, UiS, NTNU and SINTEF are gratefully acknowledged for funding and supporting this work. We thank the reviewers and editors of *Applied Rheology* for their valuable suggestions to improve the manuscript.

Bibliography

[1] Mahto V, Sharma VP: Rheological study of a water based oil well drilling fluid, J. Pet. Sci. Eng. 45 (2004) 123–128.

[2] Benyounes K, Mellak A, Benmounah A, Oubraham C: Effect of polymer concentration on the rheological properties of polyelectrolyte solutions, In: 14th SGEM GeoConference on Science and Technologies in Geology, Exploration and Mining, Surveying Geology & Mining Ecology Management (SGEM), Sofia (2014) 703–710.

[3] Elemam AE, Hussien RA, Ibrahim AA, Mohamed SA: Impacts of Polyanionic Cellulose Polymer (PAC-LV) on Drilling Fluids Properties, SUST J. Eng. Comput. Sci. JECS 16 (2015) 30–36.

[4] Kok MV, Alikaya T: Effect of Polymers on the Rheological Properties of KCl/Polymer Type Drilling Fluids, Energy Sources 27 (2005) 405–415.

[5] Olatunde AO, Usman MA, Olafadehan OA, Adeosun TA, Ufot OE: Improvement of Rheological Properties of Drilling Fluid using Locally Based Materials, Pet. Coal 54 (2012) 65–75.

[6] Razi MM, Razi FM, Saadati H: Modification of rheological and API fluid loss of bentonine-based drilling fluids using polyanionic Cellulose (PAC), In: Proceedings of the 3rd Iranian Petroleum Conference, IPEC, Teheran (2012).

[7] Ramadan A, Saasen A, Skalle P: Application of the minimum transport velocity model for drag-reducing polymers, J. Pet. Sci. Eng. 44 (2004) 303–316.

[8] Ramadan A, Skalle P, Johansen ST, Svein J, Saasen A: Mechanistic model for cuttings removal from solid bed in inclined channels, J. Pet. Sci. Eng. 30 (2001) 129–141.

[9] Noah AZ: Optimizing Drilling Fluid Properties and Flow Rates for Effective Hole Cleaning at High-Angle and Horizontal Wells, J. Appl. Sci. Res. 9 (2013) 705–718.

[10] Nguyen TN, Miska SZ, Yu M, Takach NE, Ramadan A: Experimental study of hydraulic sweeps in horizontal wells, Wiert. Nafta Gaz 27 (2010) 307–331.

[11] Rabenjafimanantsoa HA, Time RW, Saasen A: Flow regimes over particle beds - Experimental studies of particle transport in horizontal pipes, Annu. Trans. Nord. Rheol. Soc. 13 (2005) 99–106.

[12] Garcia-Hernandez AJ, Miska SZ, Yu M, Takach NE, Zettner CM: Determination of cuttings lag in horizontal and deviated wells, In: SPE Annual Technical Conference and Exhibition, Society of Petroleum Engineers, Anaheim, CA (2007).

[13] Johnsen MS: Particle transport and hole cleaning in wells during drilling, Master thesis, University of Stavanger (2014).

[14] Adari RB, Miska S, Kuru E, Bern P, Saasen A: Selecting drilling fluid properties and flow rates for effective hole cleaning in high-angle and horizontal wells, In: SPE Annual Technical Conference and Exhibition, Society of Petroleum Engineers, Dallas (2000).

[15] Sorgun M: Modeling of Newtonian fluids and cuttings transport analysis in high inclination wellbores with pipe rotation, PhD thesis, Middle East Technical University, Ankara (2010).

[16] Khatibi M, Time RW, Rabenjafimanantsoa HA: Particles Falling Through Viscoelastic Non-Newtonian Flows in a Horizontal Rectangular Channel Analyzed with PIV and PTV Techniques, J. Non-Newton. Fluid Mech. 235 (2016) 143–153.

[17] Time RW, Rabenjafimanantsoa AH: Splitting Mechanisms and Dynamics of Taylor Bubbles in Non-Newtonian Fluids in Annuli with Relevance to Gas-Kicks in Petroleum Wells, Annu. Trans. Nord. Rheol. Soc. 20 (2012) 79–88.

[18] Rabenjafimanantsoa AH, Time RW, Paz T: Dynamics of expanding slug flow bubbles in non-Newtonian drilling fluids, Annu. Trans. Nord. Rheol. Soc. 19 (2011) 69–76.

[19] Time RW, Rabenjafimanantsoa HA: Dynamics of Stagnant Taylor Bubbles in Vertical Upward Pipe Flow with Venturi Obstruction and non-Newtonian Liquids, Annu. Trans. Nord. Rheol. Soc. 23 (2015) 69–77.

[20] Bingham EC: Fluidity and plasticity, Vol. 2. McGraw-Hill Book Company, Inc. (1922).

[21] Ostwald W: Ueber die Geschwindigkeitsfunktion der Viskosität disperser Systeme, Colloid Polym. Sci. 36 (1925) 99–117.

[22] Herschel W, Bulkley R: Konsistenzmessungen von Gummi-Benzollösungen, Kolloid-Z. 39 (1926) pp 291-300.

[23] Cross MM: Rheology of non-Newtonian fluids: a new flow equation for pseudoplastic systems, J. Colloid Sci. 20 (1965) 417–437.

[24] Carreau PJ 1939-: Rheological equations from molecular network theories, 1968. (1968).

[25] Metzner AB, Reed JC: Flow of non-newtonian fluids-correlation of the laminar, transition, and turbulent-flow regions, AIChE J. 1 (1955) 434–440.

[26] Hughes TL, Jones TG, Houwen OH: Chemical characterization of CMC and its relationship to drilling-mud rheology and fluid loss, SPE Drill. Complet. 8 (1993) 157–164.

[27] Palumbo S, Giacca D, Ferrari M, Pirovano P: The development of potassium cellulosic polymers and their contribution to the inhibition of hydratable clays, In: SPE International Symposium on Oilfield Chemistry, Society of Petroleum Engineers (1989).
[28] PAC - Schlumberger Oilfield Glossary [homepage on the Internet], Available from: http://www.glossary.oilfield.slb.com/Terms/p/pac.aspx
[29] Khatibi M, Potokin N, Time RW: Experimental Investigation of Effect of Salts on Rheological Properties of Non-Newtonian Fluids, Annu. Transasctions Nord. Rheol. Soc. 24 (2016).
[30] Florjancic U, Zupancic A, Zumer M: Rheological characterization of aqueous polysaccharide mixtures undergoing shear, Chem. Biochem. Eng. Q. 16 (2002) 105–118.
[31] Vais AE, Palazoglu TK, Sandeep K p., Daubert CR: Rheological Characterization of Carboxymethylcellulose Solution Under Aseptic Processing Conditions, J. Food Process Eng. 25 (2002) 41–61.
[32] ABDELRAHIM KA, RAMASWAMY HS, DOYON G, TOUPIN C: Effects of concentration and temperature on carboxymethylcellulose rheology, Int. J. Food Sci. Technol. 29 (1994) 243–253.
[33] Benchabane A, Bekkour K: Rheological properties of carboxymethyl cellulose (CMC) solutions, Colloid Polym. Sci. 286 (2008) 1173–1180.
[34] Kulicke W-M, Reinhardt U, Fuller GG, Arendt O: Characterization of the flow properties of sodium carboxymethylcellulose via mechanical and optical techniques, Rheol. Acta 38 (1999) 26–33.
[35] Jan Schaffer (Anton Paar): Personal communication, (2017).
[36] Irgens F: Rheology and Non-Newtonian Fluids, Springer International Publishing, Cham (2014).
[37] Barnes HA: A handbook of elementary rheology, Univ. of Wales, Institute of Non-Newtonian Fluid Mechanics, Aberystwyth (2000).
[38] ISO/TC 67, SC 3: ISO 10416 : 2008 - Petroleum and natural gas industries - Drilling fluids - Laboratory testing, International Organization for Standardization (ISO) (2008).
[39] Busch A, Islam A, Martins D, Iversen FP, Khatibi M, Johansen ST, et al.: Cuttings Transport Modeling - Part 1: Specification of Benchmark Parameters with a Norwegian Continental Shelf Perspective, SPE Drill. Complet. in press (2018).
[40] API RP 13D: Rheology and Hydraulics of Oil-Well Drilling Fluids, American Petroleum Institute (API), Washington, D. C. (2010).
[41] ISO/TC 67, SC 3: ISO 10414-1 : 2008 - Petroleum and natural gas industries - Field testing of drilling fluids - Part 1 - Water-based fluids.pdf, International Organization for Standardization (ISO) (2008).
[42] Bird RB, Armstrong RC, Hassager O: Dynamics of Polymeric Liquids. Volume 1: Fluid Mechanics, Vol. 1. New York (1987).
[43] Tehrani A: Thixotropy in Water-Based Drilling Fluids, Annu. Trans. Nord. Rheol. Soc. 16 (2008).
[44] Laun HM: Prediction of Elastic Strains of Polymer Melts in Shear and Elongation, J. Rheol. 30 (1986) 459–501.
[45] Cox WP, Merz EH: Correlation of dynamic and steady flow viscosities, J. Polym. Sci. 28 (1958) 619–622.
[46] Larson RG: Constitutive equations for thixotropic fluids, J. Rheol. 59 (2015) 595–611.
[47] Wagner CE, Barbati AC, Engmann J, Burbidge AS, McKinley GH: Apparent shear thickening at low shear rates in polymer solutions can be an artifact of non-equilibration, Appl. Rheol. 26 (2016).
[48] Mezger TG: The Rheology Handbook, Vincentz Network, Hannover (2014).
[49] Laun M, Auhl D, Brummer R, Dijkstra DJ, Gabriel C, Mangnus MA, et al.: Guidelines for checking performance and verifying accuracy of rotational rheometers: viscosity measurements in steady and oscillatory shear (IUPAC Technical Report), Pure Appl. Chem. 86 (2014) 945–1968.
[50] Balestrini A, Maas A, Seheult M, Morton EK: Advances in API/ISO Standard Grade Purified Poly-Anionic Cellulose (PAC) and Drilling Grade Xanthan Gum (XG) Test Procedure and Specifications Definition, In: 2009 SPE/IADC Drilling Conference and Exhibition, Amsterdam (2009).
[51] ISO/TC 67, SC 3: ISO 13500 : 2008 - Petroleum and natural gas industries - Drilling fluid materials - Specifications and tests, International Organization for Standardization (ISO) (2008).
[52] Schiller L, Naumann A: Über die grundlegenden Berechnungen bei der Schwerkraftaufbereitung, Z Ver Dtsch Ing 77 (1933) 318–320.
[53] Singh J, Rudman M, Blackburn HM, Chryss A, Pullum L, Graham LJW: The importance of rheology characterization in predicting turbulent pipe flow of generalized Newtonian fluids, J. Non-Newton. Fluid Mech. 232 (2016) 11–21.
[54] Deshmukh SR, Sudhakar K, Singh RP: Drag-reduction efficiency, shear stability, and biodegradation resistance of carboxymethyl cellulose-based and starch-based graft copolymers, J. Appl. Polym. Sci. 43 (1991) 1091–1101.

[55] Roy A, Larson RG: A Mean Flow Model for Polymer and Fiber Turbulent Drag Reduction, Appl. Rheol. 15 (2005) 370–389.
[56] Barnes HA, Hutton JF, Walters K: An introduction to rheology, Elsevier : Distributors for the U.S. and Canada, Elsevier Science Pub. Co, Amsterdam ; New York (1989). (Rheology series).
[57] Acharya A, Mashelkar RA, Ulbrecht J: Flow of inelastic and viscoelastic fluids past a sphere - I. Drag coefficient in creeping and boundary-layer flows, Rheol. Acta 15 (1976) 454–470.
[58] Güngör N: Effect of the adsorption of surfactants on the rheology of Na-bentonite slurries, J. Appl. Polym. Sci. 75 (2000) 107–110.
[59] Oltedal VM, Werner B, Lund B, Arild Saasen, Ytrehus JD: Rheological properties of oil based drilling fluids and base oils, In: Proceedings of the ASME 2015 34th International Conference on Ocean, Offshore and Arctic Engineering OMAE2015, American Society of Mechanical Engineers, St. John's, Newfoundland (2015).
[60] Reiner M: The Deborah Number, Phys. Today 17 (1964) 62.
[61] Torsvik A, Myrseth V, Opedal N, Lund B, Saasen A, Ytrehus JD: Rheological comparison of bentonite based and KCl / polymer based drilling fluids, Annu. Trans. Nord. Rheol. Soc. 22 (2014).
[62] Benyounes K, Mellak A, Benchabane A: The Effect of Carboxymethylcellulose and Xanthan on the Rheology of Bentonite Suspensions, Energy Sources Part Recovery Util. Environ. Eff. 32 (2010) 1634–1643.
[63] Barnes HA: Thixotropy - a review, J. Non-Newton. Fluid Mech. 70 (1997) 1–33.
[64] Taghipour MA, Lund B, Sandvold I, Opedal N: Experimental Study of Rheological Properties of Model Drilling Fluids, Annu. Trans. Nord. Rheol. Soc. 20 (2012).

Figures

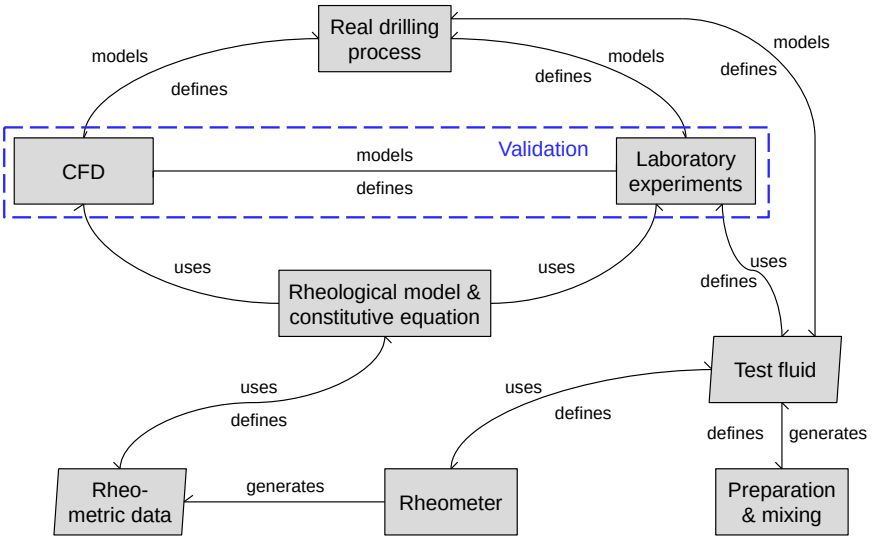

Figure 1: Overview of cuttings transport modeling via CFD and/or laboratory experiments and the role of rheometric testing.

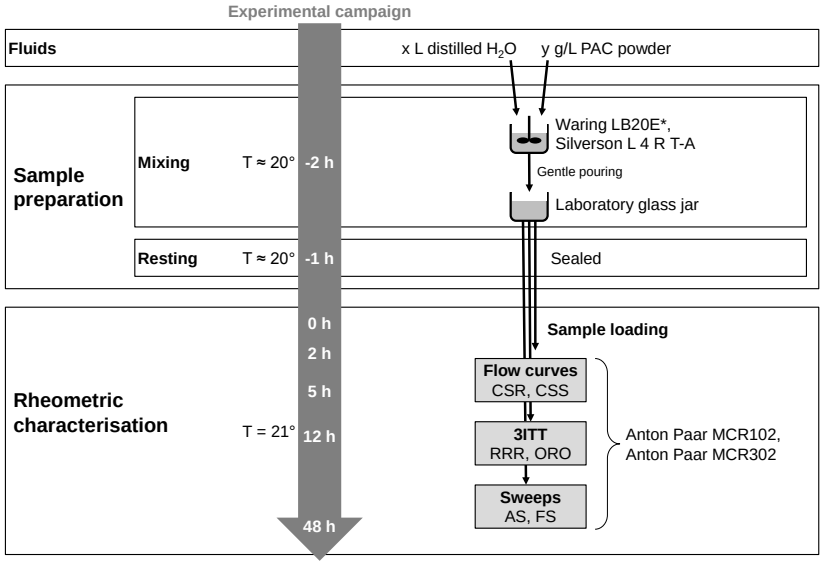

Figure 2: Test plan as applied in this study. Monitoring of natural degradation of fluid over duration of experimental campaign by obtaining flow curves at times indicated. All preparation and testing was conducted at ambient pressure, i.e. p ≈ 101325 Pa.

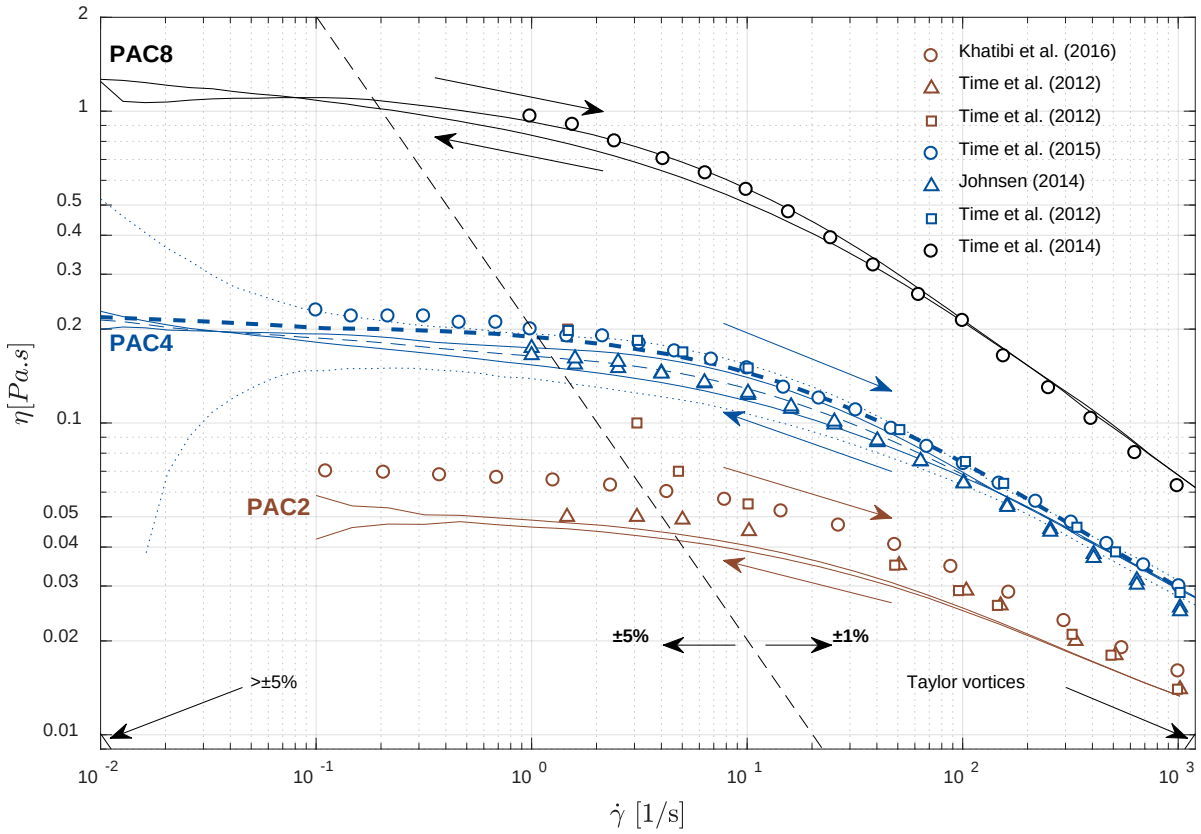

Figure 3: Flow curves (FC) for different concentrations tested and FC obtained from the literature. Solid lines are means of upward and downward sweeps, respectively (PAC4 based on 13, all others based on three consecutive measurements), the means of the two sweeps are represented by the dashed lines. Small dotted lines represent means of up-/downward sweep ± 3SD, thick dashed line represents logarithmic MPD. Colored arrows indicate direction of rheometer sweeps. The dashed black line indicates the rheometer accuracy [35] threshold as given by Eq. (4), the smaller black lines in the bottom left and right corners indicate the end of the rheometer accuracy threshold and the beginning of the Taylor vortices regime as given by Eq. (5), respectively.

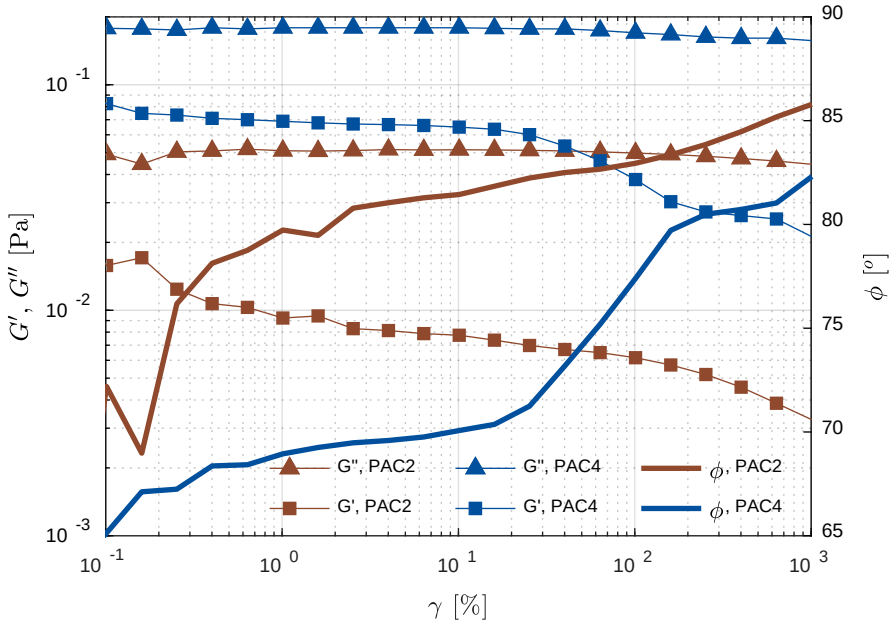

Figure 4: Amplitude Sweeps (ω = 10 rad/s), PAC2 and PAC4.

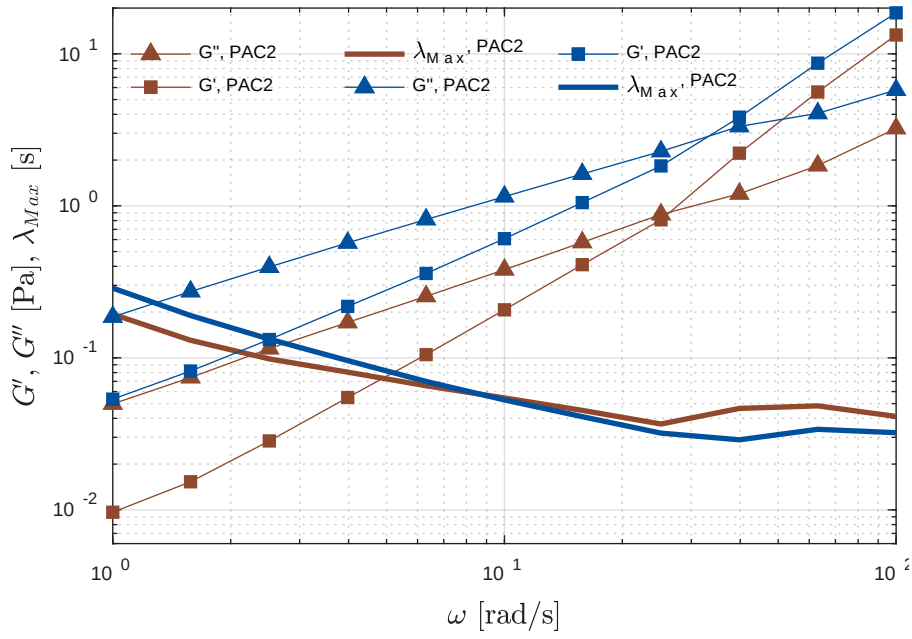

Figure 5: Frequency Sweeps (γ = 0.2%), PAC2 and PAC4.

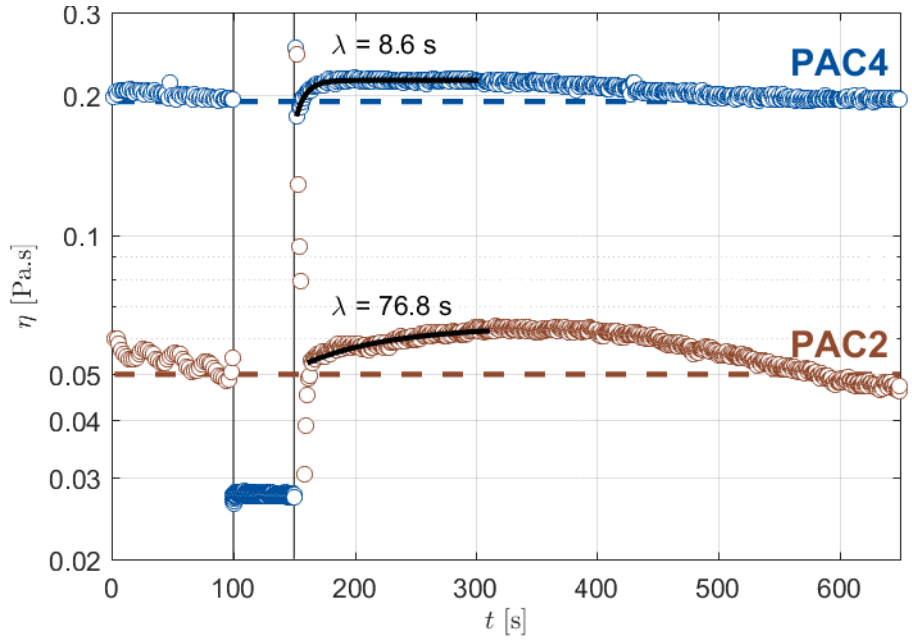

Figure 6. 3ITT-RRR, 100-50-500 test, PAC2 (partly smoothed) and PAC4 apparent viscosity η response to shear rate steps ($\dot{\gamma}$ = 0.1→1200→0.1 s^{-1}).

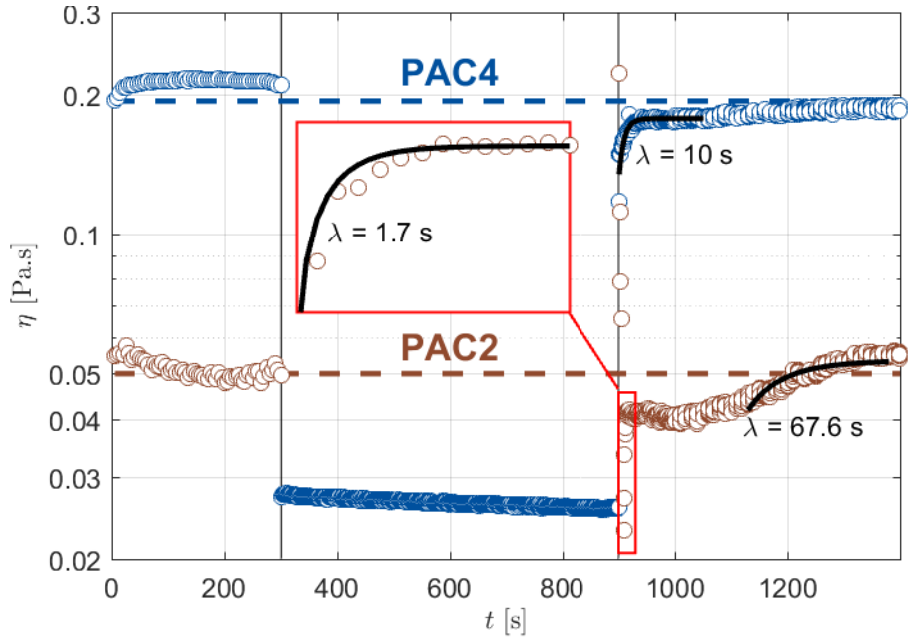

Figure 7. 3ITT-RRR, 300-600-500 test, PAC2 (partly smoothed) and PAC4 apparent viscosity η response to shear rate steps ($\dot{\gamma}$ = 0.1→1200→0.1 s^{-1}).

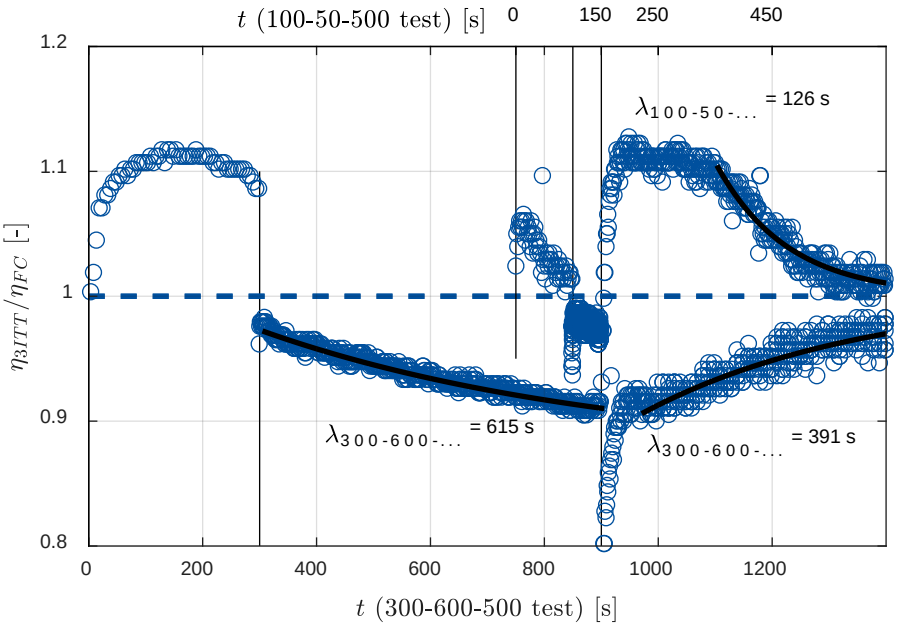

Figure 8. 3ITT-RRR, 300-600-500 test, η_{3ITT} normalized with respective FC apparent viscosity value η_{FC}.

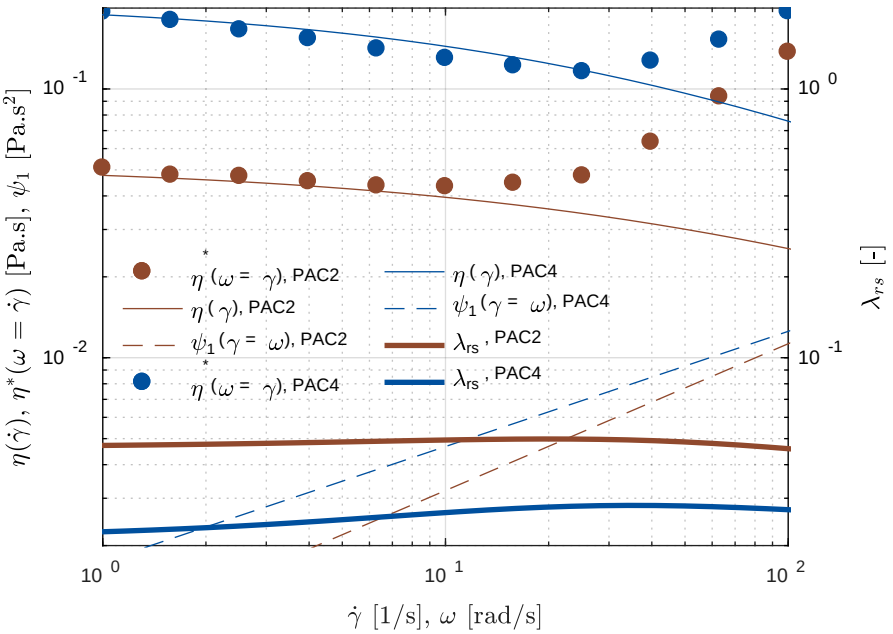

Figure 9: Cox-Merz-rule ($\eta(\dot\gamma) \approx \eta^*(\omega=\dot\gamma)$) and PAC2 and PAC4 time scales λ_{rs}, where the respective coefficients are based on PL-fits of the FNSD N_1 (here plotted as PL of the FNSC $\psi_1 = N_1/\dot\gamma^2$) and $\eta(\dot\gamma)$ via equation (10).

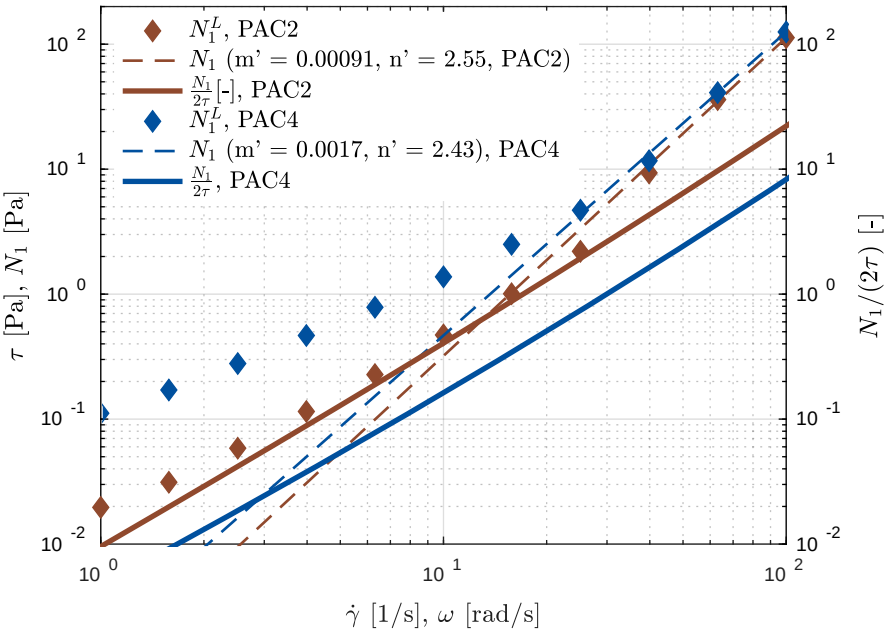

Figure 10: PAC2 and PAC4 recoverable shear $N_1/(2\tau)$, where the FNSD N_1 is based on PL fits to the FNSD $N_1^L = \psi_1\,\dot\gamma^2$ and the FNSC ψ_1 is obtained from FS data via Laun's rule [44].

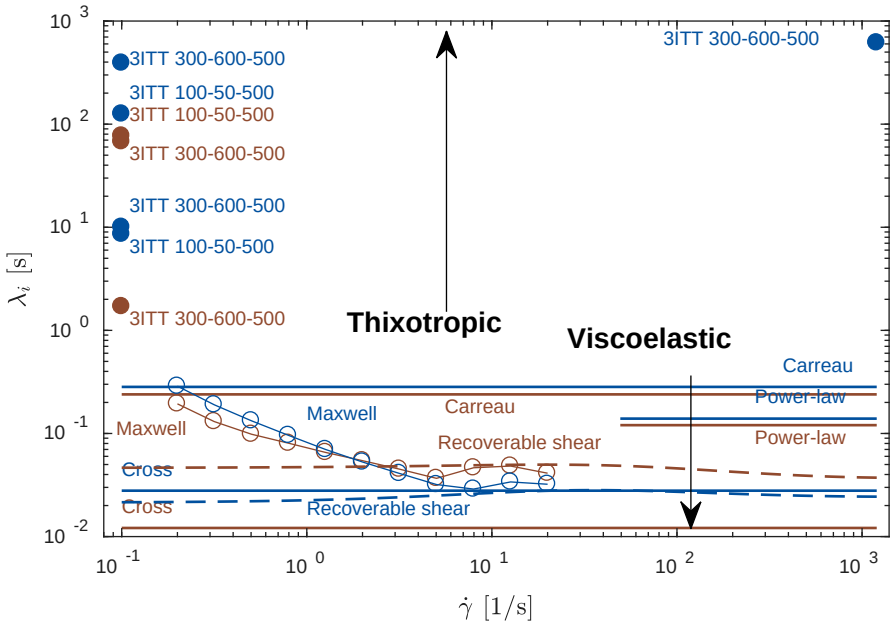

Figure 11: PAC2 and PAC4 time scales overview.

Tables

Fluid	PAC concentration			Mix. density
	[wt%]	[ppm]	[g/L]	[kg/m³]
PAC2	0.2	2000	2	998.0
PAC4	0.4	4000	4	998.2
PAC8	0.8	8000	8	999.0

Table 1. Fluid specification (T = 21°C, Solvent: Distilled H_2O).

Process steps	Waring LB20E*/	Silverson L4RT-A
Preparation	Depending on the concentration required, a pre-calculated amount of PAC granules was established using a laboratory scale.	
Addition	Running the mixer at low speeds (400-900 rpm), the PAC granules were slowly and evenly (in order to ensure all particles to become individually wetted) added to the first half of the distilled water using a spatula at the position of assumed highest shear over the mixing blades. After full addition of the PAC granules, the second half of water was gently added to the mixture.	Running the mixer at fairly high speed (3000 rpm), the PAC granules were slowly and evenly (in order to ensure all particles to become individually wetted) added to the first half of the distilled water using a spatula at the position of assumed highest shear over the mixing blades. After full addition of the PAC granules, the second half of water was gently added to the mixture.
Mixing	The mixer was set to higher speeds (3300 rpm) for half an hour.	The mixer was set to lower speeds (2000 rpm) for half an hour.
Resting	The solutions were transferred to glass jars, sealed and were left to rest at ambient temperature (T ≈ 20°) for a minimum of 1 hour prior to measurements.	The solutions were transferred to glass jars, sealed and were left to rest in a dark place at ambient temperature (T ≈ 20°) for a minimum of 48 hours prior to measurements.

Table 2: Sample preparation procedures.

Test	Anton Paar MCR102	Anton Paar MCR302
FC	Upward and downward sweeps with $\dot{\gamma}$ = 0.01…1200 s^{-1} (typical cuttings transport shear rate range[8]) in a CSR mode with a constant measurement point duration[9] (MPD) Δt = 5 s.	As Anton Paar MCR102, but with logarithmically decreasing MPD Δt = 120…2 s log for the upward sweep and vice-versa for the downward sweep.
AS	Fixed angular frequency ω = 10 rad/s and logarithmically increasing strain γ = 0.1…1000%.	
FS	Fixed strain γ = 0.02% and logarithmically increasing angular frequency ω = 0.1…100 rad/s.	
3ITT	Low rotational shear intervals $\dot{\gamma}$ = 0.1 s^{-1} and an intermediate high rotational shear interval with $\dot{\gamma}$ = 1200 s^{-1} for 50 s and 600 s.	

Table 3: Rheometer settings.

[8] In cuttings transport problems, the lower shear rate range corresponds to the hydrodynamics of particles settling in a stagnant fluid, whereas the higher shear-rate range corresponds to the hydrodynamics of the main flow field, i.e. annular flow.

[9] Measurement point duration (MPD) is the time interval it takes for the rheometer to obtain an apparent viscosity reading for a particular shear rate. According to Anton Paar, the first two thirds of an arbitrary MPD are dedicated to reduce of any dynamics (flow field or microstructural) in the sample. The actual data sampling is then conducted in the last third of the MPD assuming an equilibrium of both flow field and microstructure of the sample [35].

Fluid	Model	μ_0 [Pa·s]	μ_∞ [Pa·s]	λ [s]	n [-]	R^2	SSE
	PL	0.0491	0	0.12	0.731	0.999	$3.71 \cdot 10^{-7}$
PAC2	**Carreau**	0.0491	0.001	0.239	0.771	0.99	$3.82 \cdot 10^{-5}$
	Cross	0.0525	0.001	0.012	0.516	-Inf	Inf
	PL	0.202	0	0.139	0.617	0.998	$1.11 \cdot 10^{-5}$
PAC4	**Carreau**	0.202	0.001	0.282	0.689	0.981	$3.10 \cdot 10^{-3}$
	Cross	0.212	0.001	0.029	0.574	0.999	$2.38 \cdot 10^{-4}$

Table 4: Model coefficients for PL ($\dot{\gamma} > 48\ s^{-1}$), Carreau and Cross models, equations (6)-(8) for PAC2 and PAC4 data with goodness-of-fit R^2 and sum of squared errors SSE.